

APEX: A Decoupled Memory-based Explorer for Asynchronous Aerial Object Goal Navigation

Daoxuan Zhang¹ Ping Chen¹ Xiaobo Xia² Xiu Su³ Ruichen Zhen⁴
 Jianqiang Xiao¹ Shuo Yang^{1✉}

¹ Harbin Institute of Technology, Shenzhen ² National University of Singapore

³ Central South University ⁴ Meituan Academy of Robotics Shenzhen, Meituan

2023311529@stu.hit.edu.cn shuoyang@hit.edu.cn

Abstract

Aerial Object Goal Navigation, a challenging frontier in Embodied AI, requires an Unmanned Aerial Vehicle (UAV) agent to autonomously explore, reason, and identify a specific target using only visual perception and language description. However, existing methods struggle with the memorization of complex spatial representations in aerial environments, reliable and interpretable action decision-making, and inefficient exploration and information gathering. To address these challenges, we introduce APEX (Aerial Parallel Explorer), a novel hierarchical agent designed for efficient exploration and target acquisition in complex aerial settings. APEX is built upon a modular, three-part architecture: 1) Dynamic Spatio-Semantic Mapping Memory, which leverages the zero-shot capability of a Vision-Language Model (VLM) to dynamically construct high-resolution 3D Attraction, Exploration, and Obstacle maps, serving as an interpretable memory mechanism. 2) Action Decision Module, trained with reinforcement learning, which translates this rich spatial understanding into a fine-grained and robust control policy. 3) Target Grounding Module, which employs an open-vocabulary detector to achieve definitive and generalizable target identification. All these components are integrated into a hierarchical, asynchronous, and parallel framework, effectively bypassing the VLM’s inference latency and boosting the agent’s proactivity in exploration. Extensive experiments show that APEX outperforms the previous state of the art by +4.2% SR and +2.8% SPL on challenging UAV-ON benchmarks, demonstrating its superior efficiency and the effectiveness of its hierarchical asynchronous design. Our source code is provided in [GitHub](#).

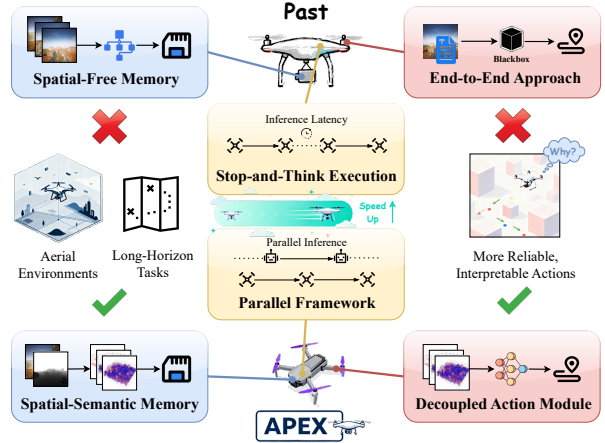


Figure 1. **APEX addresses three critical limitations in prior works.** 1) Memory: APEX employs a rich 3D dynamic map for robust spatial reasoning. 2) Decision-Making: APEX uses decoupled modules, separating semantic understanding from action generation for more reliable and interpretable control. 3) Efficiency: APEX employs a parallel and asynchronous framework that mitigates inference latency and boosts exploration proactivity.

1. Introduction

The rapid increase in the use of Unmanned Aerial Vehicles (UAVs) [48] and Vision-Language Models (VLMs) [9, 21, 51] are driving advancements in aerial embodied intelligence [32, 38]. The combination of these technologies has greatly advanced Vision-Language Navigation (VLN) [10, 43, 54], traditionally focused on indoor, ground-based scenarios, into the challenging domain of Aerial Vision-Language Navigation (AVLN) [8, 17, 24, 47]. This transition represents a significant leap in complexity, moving from constrained 2D planes to complex 3D spaces. However, a critical limitation of many existing AVLN frame-

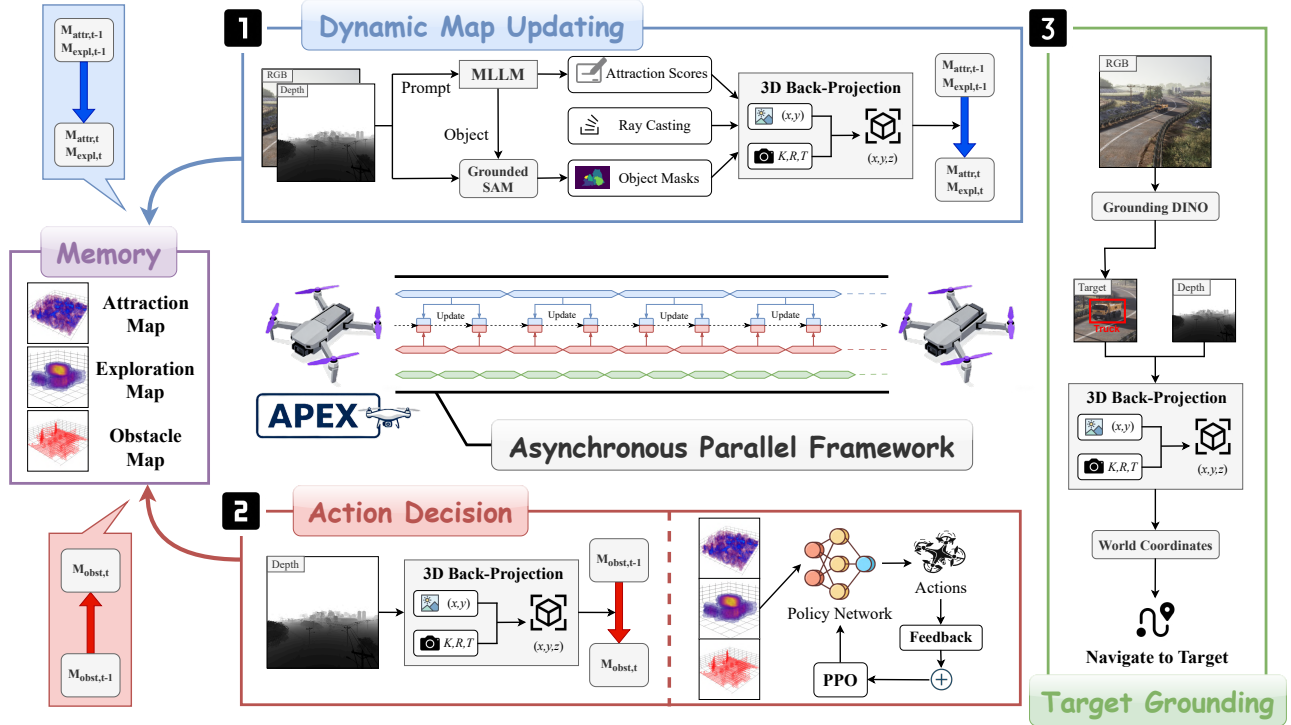


Figure 2. **The overall framework of APEX.** Module 1 extracts and integrates visual information into 3D dynamic spatio-semantic maps, serving as the agent’s memory. Module 2 utilizes the stored information from Module 1 for action decision-making via an RL-based model. Module 3 continuously performs object detection on visual observations to obtain precise target locations. The three modules are integrated into a hierarchical asynchronous parallel system.

works is their reliance on fine-grained, step-by-step language instructions [6, 22, 42]. Such detailed guidance is often impractical to obtain in real-world settings and fundamentally constrains the agent’s autonomy, limiting the scalability and applicability of these systems in open-ended exploration tasks [53, 57].

To address this limitation, we focus on a more challenging and practical task: Aerial Object Goal Navigation (Aerial ObjectNav) [44]. In this paradigm, the UAV agent is tasked with locating a specific object described by a high-level textual cue (*e.g.*, “a red tent”) using only its onboard visual sensors. This requires the agent to autonomously explore the environment, reason about spatial relationships, and actively search for the target, mirroring a more realistic operational scenario.

As shown in Fig. 1, developing an Aerial ObjectNav agent faces three major challenges that are insufficiently addressed by prior work:

1) **Ineffective Spatial-Temporal Information Integration.** The transition from ground to aerial navigation brings an exponential increase in the volume and complexity of perceptual information [18, 23, 37]. Operating in expansive 3D environments, agents must execute long-horizon

tasks that require effective long-term memory. However, many existing approaches [4, 56] fail to integrate historical observations with complex spatial information, resulting in inefficient exploration and repeated errors. Other works [19, 26, 45] employ abstract memory structures like topological maps, but these representations often sacrifice crucial geometric and metric fidelity, impairing the agent’s ability to perform fine-grained reasoning and planning in complex aerial terrains.

2) **The Gap Between Semantic Understanding and Actionable Control.** While VLMs exhibit remarkable proficiency in grounding language to visual concepts, a significant gap exists between their high-level semantic reasoning and the low-level action control required for navigation [59]. Contemporary methods [27, 34, 39, 40] attempt to use a VLM as an end-to-end decision-maker, directly mapping visual-linguistic inputs to actions. This approach not only demands vast quantities of high-quality demonstration data but also results in policies that are often unstable, unreliable, and lack interpretability, making them unsuitable for safety-critical applications, especially in aerial environments.

3) **Computational Latency and Real-Time Constraints.** The high computational cost of running large

VLMs presents a critical challenge to real-world deployment [7]. Most existing frameworks [12, 44, 52] overlook the severe time costs, implicitly assuming a “stop-and-think” execution model. This latency prevents the smooth, continuous motion necessary for efficient and practical UAV operation, making these systems unsuitable for real-time missions.

To overcome these challenges, we propose APEX (Aerial Parallel Explorer), a novel hierarchical agent designed for efficient aerial object navigation. APEX’s core contribution lies in decoupling the complex navigation task into three specialized modules: a Dynamic Spatio-Semantic Mapping module, an RL-based Action Decision module, and a Target Grounding module for precise and definitive target identification. By integrating these components within an asynchronous, parallel framework, APEX enables effective long-horizon planning in complex aerial environments, enhances the reliability and interpretability of decision-making, and achieves high operational efficiency.

Before delving into details, our contributions are summarized as follows:

- We propose a novel dynamic 3D mapping mechanism specifically for aerial object navigation, which enhances the agent’s ability to integrate and maintain complex spatial information over long-horizon tasks in expansive 3D environments.
- We demonstrate the advantages of a modular, decoupled design for planning and control in Aerial Object-Nav. Through extensive experiments, we show that this approach surpasses end-to-end models in terms of reliability and interpretability.
- We introduce a multi-module, asynchronous parallel architecture. Our experiments demonstrate that this framework improves exploration efficiency in Aerial Object Navigation, which is often overlooked in prior work. This paradigm sets a new standard for building practical and responsive aerial agents.

2. Related Work

2.1. Object Goal Navigation

Object Goal Navigation is an Embodied AI task where an agent must autonomously find a target object in an unseen environment [1]. Researches in this area, sped up by photorealistic simulators like Matterport3D [5] and AI2-THOR [15], has evolved from classical modular pipelines to learning-based paradigms. To improve generalization, many modern methods employ imitation learning (IL) or reinforcement learning (RL) to train end-to-end navigation policies [11, 13, 30, 58].

The capabilities of Multimodal Large Language Models (MLLMs) have recently revolutionized this domain by equipping agents with powerful commonsense reasoning

[20, 49]. For instance, NavGPT-2 [60] aligns visual and linguistic information within a frozen LLM to bridge the performance gap between generalist LLM agents and specialized navigation models. Similarly, VoroNav [41] leverages an LLM to interpret semantic and topological information from a dynamically map, enabling more efficient zero-shot exploration by reasoning about navigational waypoints.

However, the challenges of ObjectNav are significantly amplified when transitioning from ground to aerial navigation [12, 14]. The complexity of vast 3D environments places greater demands on an agent’s perception and planning. To this end, UAV-ON [44] established a large-scale simulation benchmark for aerial ObjectNav, while PRPSearcher [12] proposed a 3D semantic map-based framework to improve spatial understanding. Despite this progress, developing an agent that is both efficient and reliable for long-horizon aerial tasks remains a critical open problem. To address this, our Dynamic-Mapping Module improves the agent’s abilities of memorizing in aerial navigation, while the Action Decision Module enables more reliable action outputs.

2.2. Aerial Vision-Language Navigation

Inspired by the advancements in ground-based VLN [2, 16], Aerial Vision-Language Navigation (AVLN) has recently emerged as a challenging new frontier, extending embodied navigation to the complexities of 3D aerial environments [35, 36, 55]. Foundational works like AerailVLN [24] provide a dedicated simulator, a large-scale dataset, and a baseline method. Following this, TravelUAV [40] introduced continuous control for more realistic simulation and proposed an end-to-end LLM-based agent for aerial navigation. Recent improvements have focused on specific modules: To enhance long-horizon task performance, SkyVLN [19] and NavAgent [26] introduced topological map architectures as the agent’s memory modules, abstracting spatial relationships for efficient planning. To boost the generalization and adaptability of the VLM backbone, FlightGPT [4] employs a two-stage training pipeline, including Supervised Finetuning and GRPO algorithm. To improve spatial reasoning, CityNavAgent [52] enhanced the agent’s understanding of 3D geometry by projecting visual information onto point clouds.

However, existing AVLN methods exhibit notable limitations. First, their performance is often contingent upon high-quality, detailed language instructions, which may not be available in more open-ended, goal-driven scenarios. Furthermore, a critical and under-explored issue is the loss of complex spatial information in their memory module designs. For instance, while topological maps are effective for high-level planning, they often discard the precise geometric details essential for fine-grained maneuvering and obstacle avoidance in cluttered 3D spaces. We address these

problems with a system that navigates using simple goal descriptions, supported by dynamic 3D maps that retain crucial spatio-semantic information.

3. Methodology

3.1. Task Formulation

We formulate the Aerial Object Goal Navigation task as a sequential decision-making process. At each timestep t , the agent receives a visual observation O_t , its self state S_t , and a text description D . In a basic setting, the agent’s policy, denoted by π , maps the current sensory inputs and the goal description to an action A_t from a discrete action space \mathcal{A} :

$$A_t = \pi(O_t, S_t, D). \quad (1)$$

For long-horizon tasks that require efficient exploration and recall of the environment, we introduce a memory module MEM to aggregate spatial-semantic information. The module updates the memory state from MEM_{t-1} by incorporating new information from O_t and S_t :

$$MEM_t = f_{\text{update}}(MEM_{t-1}, O_t, S_t). \quad (2)$$

With this memory-augmented framework, the agent’s policy now makes decisions on the accumulated memory:

$$A_t = \pi(O_t, S_t, MEM_t, D). \quad (3)$$

The ultimate goal of the agent is to reach the target efficiently, formulated as finding a policy π^* that maximizes the success metric.

3.2. Overview

As illustrated in Fig. 2, the APEX architecture is designed to support efficient Aerial ObjectNav by addressing three core challenges of the task. Each of them is handled by a dedicated module:

Dynamic Spatio-Semantic Mapping Module. To navigate purposefully, the agent first needs to build a model of the world. This module creates and maintains this model by processing visual and textual inputs from an MLLM [3] and a segmentation model [31]. It generates three dynamic 3D maps: the Attraction Map to guide the agent toward the goal, the Obstacle Map for safety, and the Exploration Map to ensure active exploration.

RL-based Action Decision Module. With a clear understanding of the environment, the agent must then choose its next action. This module uses the generated maps as input for a Proximal Policy Optimization (PPO) [33] policy network. The network learns to translate high-level spatial intelligence into low-level actions, enabling effective and reliable movements.

Target Grounding Module. To solve the “last-mile” problem of target identification, the agent needs to be certain

that it has found the correct object. This module uses a dedicated object detector [25] to confirm the target’s location.

These modules operate in a parallel asynchronous framework, ensuring high efficiency and overcoming latency bottlenecks for smooth exploration. The algorithm flow is provided in Appendix A.

3.3. 3D Dynamic Grid-based Map

As illustrated in Fig. 3a, our method utilizes a 3D grid-based map M as a persistent memory carrier, which is dynamically updated with spatio-semantic information at each timestep. This process involves two key stages: 3D back-projection and map generation.

3D Back-projection. Given a depth image, this process back-projects the 2D pixel grid into a 3D point cloud in the world frame. This transformation uses the camera intrinsics K , per-pixel depth values, and the current state of the agent S_t . Each resulting 3D point is then discretized to identify its corresponding grid index in the map M . We refer to this entire pipeline as the Reconstruction Projector, $\text{RP}(\cdot)$.

Attraction Map Generation. For effective Object Goal Navigation, the agent must infer which regions are promising for finding the target object. To this end, we introduce the concept of an object-centric attraction map, M_{attr} , a channel within our main map M . This map quantifies the semantic relevance of observed objects to the navigation goal. The generation process begins by leveraging MLLM’s advanced capabilities in visual grounding and common-sense reasoning [3]. Given the current observation O_t and the goal description D , the MLLM identifies N distinct objects, outputting their text captions c_1, c_2, \dots, c_N and the corresponding attraction scores s_1, s_2, \dots, s_N . A higher score s_i indicates a stronger semantic link between the object c_i and the target. We denote this process as $\text{CAP}(\cdot)$:

$$\{(c_i, s_i)\}_{i=1}^N = \text{CAP}(O_t, D). \quad (4)$$

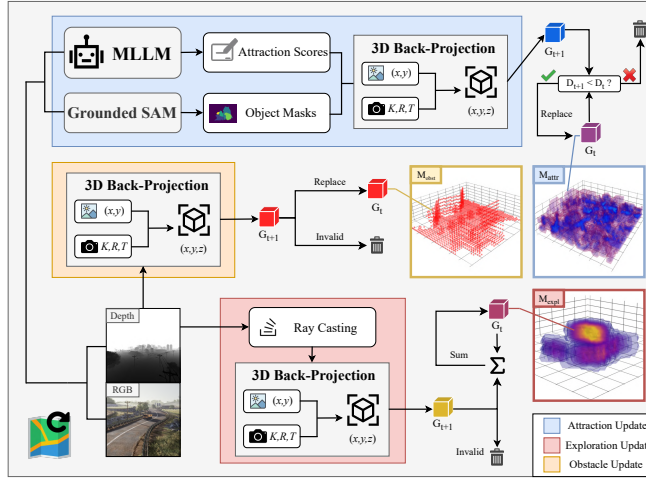
Subsequently, we employ an open-vocabulary segmentation model [31] to obtain a pixel mask $Mask_i$ for each caption c_i , denoted as $\text{SEG}(\cdot)$:

$$Mask_i = \text{SEG}(O_t, c_i). \quad (5)$$

Finally, the attraction map M_{attr} is updated by projecting these semantic masks into the 3D grid. For each voxel v in the map, the update follows two rules:

- **Majority Ownership:** The voxel is claimed by the object i^* that projects the most pixels into it.
- **Closest Observation First:** The voxel’s score is updated only if the new observation is geometrically closer than any prior observation.

Let s_{new} and d_{new} be the attraction score and minimum depth of the pixels from the winning object i that map to



(a) **3D Dynamic Map Updating.** The module processes RGB-D input to update three maps with specific rules: 1) Attraction Map: A grid's score is updated only if the current observation is geometrically closer. 2) Exploration Map: Scores from new observations are added to existing ones. 3) Obstacle Map: All grids with detected obstacles are marked as occupied.

Figure 3. Detailed architecture of the Dynamic Map Module and the Asynchronous Parallel Framework.

voxel v . The update rule for the attraction score $M_{\text{attr}}(v)$ and its associated minimum depth $M_{\text{depth}}(v)$ is:

$$\begin{cases} M_{\text{attr}}(v) \leftarrow s_{\text{new}} & \text{if } d_{\text{new}} < M_{\text{depth}}(v). \\ M_{\text{depth}}(v) \leftarrow d_{\text{new}} & \end{cases} \quad (6)$$

This ensures that the map robustly represents the most relevant and reliable information from the agent's perspective.

Exploration Map Generation. To incentivize the agent to explore unknown regions and gather more environmental information, we maintain an Exploration Map M_{expl} . This channel quantifies the observation density of each spatial region, representing an ‘‘exploration score’’.

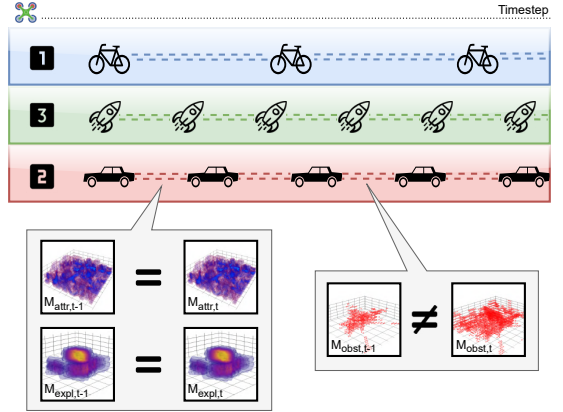
The map is updated at each timestep t using a ray casting approach. For the set of 3D world points P_w from the current depth observation, we cast a set of rays \mathcal{R} originating from the camera's position t_t towards each point P_w . The set of all voxels traversed by a single ray r , denoted as $V(r)$, is identified using a 3D voxel traversal algorithm. The union of these sets constitutes all currently visible voxels:

$$\mathcal{V}_{\text{visible}} = \bigcup_{r \in \{\mathcal{R}\}} V(r). \quad (7)$$

For each voxel $v \in \mathcal{V}_{\text{visible}}$, we calculate an exploration gain that decays exponentially with its distance from the agent. The incremental update, ΔM_{expl} , is calculated as:

$$\Delta M_{\text{expl}}(v) = \exp(-\lambda \cdot \|p_v - t_t\|_2), \quad (8)$$

where p_v is the center of voxel v , and λ is the decay rate.



(b) **Asynchronous Parallel Framework.** The agent's modules operate in parallel at different frequencies. Since the Map Update module runs slower than the Action Decision module, the Obstacle Map input for the policy is always updated between consecutive timesteps, while the Attraction and Exploration Maps may remain the same.

This incremental value is then accumulated into the map:

$$M_{\text{expl},t}(v) \leftarrow M_{\text{expl},t-1}(v) + \Delta M_{\text{expl}}(v). \quad (9)$$

This mechanism encourages the agent to prioritize navigating towards less observed regions.

Obstacle Map Generation. To enhance safe navigation and path planning, we also construct an Obstacle Map, M_{obst} . This map provides a persistent representation of occupied space. It is populated directly by the 3D Back-Projection process $\text{RP}(\cdot)$. Any voxel that contains one or more back-projected points from the depth map is marked as an obstacle. The update rule for a voxel v is simply:

$$M_{\text{obst}}(v) \leftarrow 1 \quad \text{if } v \text{ contains any } P_w. \quad (10)$$

3.4. RL-based Action Decision Module

The Action Decision Module employs a policy network, trained with the Proximal Policy Optimization (PPO) algorithm, to map the constructed 3D maps to low-level control actions. This process includes feeding three distinct 3D maps into three separate CNN feature extractors. The resulting feature vectors are then concatenated into a unified representation, which is shared by both the actor and critic networks that form the core of the policy network. This map-based approach enhances the policy's reliability and interpretability compared to end-to-end methods. To inject navigation priors and improve training efficiency, we design a composite reward function, R_t , which is a weighted sum of several components:

Sparse Reward. These rewards are given only at the end of an episode to signify ultimate success or failure.

- A large positive reward, R_{success} , is given if the agent navigates to within a threshold distance of the target.
- A large negative reward, R_{penalty} , is given for terminal states such as collisions or flying out of bounds.

Attraction Reward. This dense reward encourages the agent to leverage the semantic guidance from the Attraction Map. At each step t , the reward is calculated by summing the attraction scores of all observed voxels, weighted by a linear distance decay. For the set of visible voxels $\mathcal{V}_{\text{visible}}$ within a distance threshold d_{thresh} , the reward is:

$$R_{\text{attr}} = \sum_{v \in \mathcal{V}_{\text{visible}}} M_{\text{attr}}(v) \cdot \left(1 - \frac{\|p_v - t_t\|_2}{d_{\text{thresh}}}\right), \quad (11)$$

where $M_{\text{attr}}(v)$ is the attraction score of voxel v , p_v is its world coordinate, t_t is the agent’s position at time t , and the term in parentheses provides the linear decay. This reward incentivizes the agent to move towards and observe regions with high semantic relevance to the target.

Exploration Reward. This dense reward incentivizes the agent to explore unknown areas to gather more information. It is inversely proportional to the voxel’s current exploration score in M_{expl} :

$$R_{\text{expl}} = \sum_{v \in \mathcal{V}_{\text{visible}}} (\epsilon - M_{\text{expl}}(v)) \cdot \left(1 - \frac{\|p_v - t_t\|_2}{d_{\text{thresh}}}\right), \quad (12)$$

where ϵ represents the saturation point for exploration.

Finally, the total reward at each timestep t is the weighted sum of these components:

$$R_t = R_{\text{attr}} + \alpha R_{\text{expl}} + R_{\text{spar}}, \quad (13)$$

where α balances the scale of the attraction reward and the exploration reward.

3.5. Target Grounding Module

While the 3D map guides the agent to the general vicinity of the target, the Target Grounding Module is responsible for the final, precise localization. This module operates in parallel with other components, continuously scanning each visual observation to detect the target.

At each step in this phase, the agent employs an open-vocabulary object detector, $\text{GD}(\cdot)$, on its current RGB observation O_t to find instances matching the goal description D [25]. The detector outputs a set of candidate bounding boxes and their associated confidence scores:

$$\{\text{bbox}_j, \text{conf}_j\}_{j=1}^K = \text{GD}(O_t, D). \quad (14)$$

If the highest confidence score exceeds a predefined threshold, the target is considered successfully grounded. The precise 3D world coordinate of the target P_{target} will be computed by the Reconstruction Projector $\text{RP}(\cdot)$.

3.6. Asynchronous Parallel Framework

To address the computational bottleneck imposed by large-scale VLM inference, we integrate our modules into an asynchronous parallel framework, which is illustrated in Fig. 3b. The Attraction Map and Exploration Map serve as shared data structures that mediate information transfer between different modules, which operate at varying frequencies. The framework consists of three main components, ordered from lowest to highest operational frequency:

Dynamic Map Module. This module operates at a lower frequency and is responsible for the most computationally intensive tasks. It runs the VLM-based inference to generate attraction scores and performs ray casting to compute exploration gains. The resulting updates are asynchronously written to the shared Attraction Map and Exploration Map.

Action Decision Module. Running at the agent’s main control frequency, this module is responsible for real-time navigation. At each action step, it updates the Obstacle Map using the latest sensor data, without time-consuming processes. Then it reads the most recent versions of the Attraction Map and Exploration Map from the shared memory. These three maps collectively inform the action policy, ensuring that even if the semantic guidance is slightly stale, the agent can always navigate safely based on up-to-the-minute obstacle information.

Target Grounding Module. This module also operates at a high frequency, continuously applying the open-vocabulary detector $\text{GD}(\cdot)$ to the RGB observations. This high-rate execution maximizes the probability of detecting the target as soon as it becomes visible, without being constrained by the slower semantic mapping cycle.

4. Experiment

4.1. Experiment Settings

Dataset and Environment. We evaluate our proposed method using the UAV-ON benchmark [44]. This recently proposed benchmark is specifically designed for the Aerial ObjectNav task, providing a challenging and realistic simulation environment. It features 14 photorealistic, large-scale outdoor environments and comprises a total of 10,000 navigation episodes, split for training and testing. In each episode, the agent is tasked with autonomously navigating to a target object based on a given textual description.

Evaluation Metrics. We employ four standard metrics widely used in embodied navigation tasks to provide evaluations of navigation accuracy and path efficiency. Success Rate (SR) measures the percentage of episodes where the agent stops within a predefined distance threshold. Navigation Error (NE) is the average final Euclidean distance between the agent’s position and the target’s center at the end of each episode. Oracle Success Rate (OSR) measures success assuming an oracle stops the agent at the point along

Table 1. **Comparison with Baselines.** APEX achieves SOTA performance across various types of agents, including basic methods, ground navigation, and aerial navigation techniques.

Method	Seen				Unseen				Overall			
	SR↑	NE↓	OSR↑	SPL↑	SR↑	NE↓	OSR↑	SPL↑	SR↑	NE↓	OSR↑	SPL↑
RE	1.12	32.75	3.37	0.62	0.0	28.45	9.68	0.0	0.83	31.64	5.00	0.46
FBE [46]	4.49	66.02	11.24	2.57	6.45	63.52	12.90	6.45	5.00	65.38	11.67	3.5
MLLM-N [3]	0.0	30.39	3.37	0.0	3.23	29.83	12.88	3.23	0.83	30.25	5.83	0.83
CLIP-H [44]	6.74	46.38	12.36	4.58	3.23	49.51	16.13	3.67	5.83	47.19	13.33	4.34
L3MVN-Z [50]	8.99	61.64	15.73	6.57	9.69	63.07	16.12	9.68	9.17	62.01	15.83	7.37
TRAVEL [40]	6.74	56.66	13.48	4.82	9.68	53.12	16.15	7.60	7.48	55.75	14.17	5.54
AOA-F [44]	7.87	47.68	17.98	4.21	6.45	48.57	16.09	3.98	7.50	47.90	17.50	4.15
APEX	12.36	55.59	19.10	9.13	16.13	51.74	22.58	13.03	13.33	54.59	20.00	10.14

its trajectory that is closest to the target. Success-weighted Path (SPL) evaluates both success and efficiency by penalizing inefficient paths, weighting the success rate by the ratio of the optimal path length to the agent’s actual path length.

Baselines. To demonstrate the effectiveness of APEX, we compare it against a comprehensive set of baselines spanning different categories, including basic methods, ground navigation, and other aerial navigation techniques.

- **Random Exploration:** A naive agent that selects actions randomly at each timestep until the stop action is chosen.
- **Frontier-based Exploration [46]:** A classic exploration method without leveraging semantic information.
- **MLLM-Direct Navigation [3]:** An end-to-end approach where MLLM directly maps raw egocentric observations and the target description to actions.
- **CLIP-H [44]:** This method uses CLIP [28] to compute the similarity between observations and the textual goal, guiding the agent towards semantically relevant areas.
- **L3MVN-Zeroshot [50]:** A novel method for ground-based ObjectNav. It uses an MLLM to fuse semantic information with a frontier map for navigation decisions.
- **TravelUAV [40]:** A recent LLM-based framework designed for the AVLN task. To adapt to the experimental setup, the model’s action outputs were discretized.
- **AOA-F [44]:** An Aerial ObjectNav method that processes and feeds the target description, RGB observations, and depth observations into an LLM to generate actions.

RL Training. The policy network in our Action Decision Module maps 3D grid-based maps to discrete actions. We employ the Proximal Policy Optimization (PPO) algorithm for training this policy. PPO is widely used in navigation tasks because of its stability and strong performance [33], making it a reliable choice for our work. Our model is trained on a set of 36 tasks, comprising 4 distinct tasks across 9 environments. To accelerate training, we use 4 parallel environments, with each operating on a different map to enhance data diversity. Within each environment,

Table 2. Comparison of Efficiency and Security.

Method	Step Latency (s)	Safe Dist. (m)
L3MVN-Z	1.26	330.64
TRAVEL	1.71	223.17
AOA-F	5.29	212.36
APEX	0.97	345.51

the agent cycles through the map’s designated tasks. For each task, the agent collects experience over 10 consecutive episodes before proceeding to the next.

To enhance training stability, we adopt a two-stage training approach. Initially, a goal-agnostic exploration policy is pretrained using only the exploration reward R_{expl} and the terminal penalty R_{penalty} . This helps the agent establish a robust foundation for safe navigation and obstacle avoidance. Subsequently, this model is fine-tuned by introducing the attraction reward R_{attr} and the success reward R_{success} , guiding the policy to leverage semantic cues from the Attraction Map for efficient, goal-directed navigation. This curriculum effectively decouples the learning of general navigation skills from task-specific behaviors, fostering a final policy that balances exploration and exploitation. More training details are provided in Appendix D.

4.2. Experimental Results

Comparison with Baselines. Tab. 1 presents the comparative results of APEX and the baseline methods across four evaluation metrics. Among the basic methods, Frontier-based Exploration (FBE) significantly outperforms Random Exploration, demonstrating the fundamental benefit of systematic exploration over naive behavior. VLM-based methods, such as CLIP-H, highlight how the semantic understanding of visual scenes can effectively guide the agent. Similarly, TravelUAV, an AVLN method, also shows strong performance, but its framework is tailored for detailed lin-

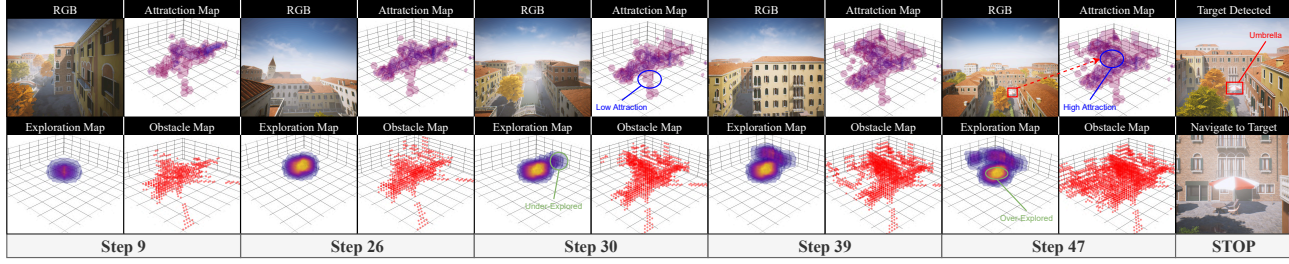


Figure 4. A case study of the APEX agent navigating to the target “Umbrella”. The figure shows the dynamic integration of the Attraction, Exploration, and Obstacle Maps in the mission, leading to successful navigation. More visualized results are demonstrated in Appendix B.

Table 3. Effect of the attraction-exploration trade-off parameter α .

α	SR↑	NE↓	OSR↑	SPL↑
0.05	5.83	29.11	9.17	5.28
0.1	9.17	41.92	15.83	8.23
0.2	13.33	54.59	20.00	10.14
0.5	11.67	58.55	15.83	9.65
0.8	12.50	62.27	16.67	11.45
1.0	7.50	66.44	13.33	4.85

guistic instructions. Additionally, L3MVN, a method for ground-based ObjectNav, also delivers highly competitive results, underscoring the power of fusing semantic information with spatial maps. However, its performance is constrained by its design, which is not optimized for the complexities of 3D aerial environments. Our proposed method, APEX, establishes a new state-of-the-art on this benchmark, achieving a 4.16% improvement in Success Rate (SR) and a 2.77% improvement in Success-weighted Path Length (SPL), while also attaining the highest Oracle Success Rate (OSR). Regarding the higher Navigation Error (NE), we attribute this to the agent’s proactive exploration strategy, which can lead to a greater final distance from the target in the subset of unsuccessful episodes.

Efficiency and Security. Tab. 2 compares the operational efficiency and safety of APEX against three top-performing baselines. Our method achieves the lowest step latency (the time between consecutive actions), demonstrating that our Asynchronous Parallel Framework effectively boosts exploration efficiency. Furthermore, APEX attains the highest average safe distance, a measure of collision-free exploration capability, showing the enhanced navigation reliability provided by our RL-based Action Decision Module.

4.3. Ablation Study

To validate the contributions of key components in APEX, we conduct a series of ablation studies.

First, we investigate the impact of the reward balancing parameter α in our RL-based Action Decision Module. This

Table 4. Ablation Study of Core Modules.

Method	SR↑	NE↓	OSR↑	SPL↑
w/o 3D-Map	1.67	45.62	4.17	0.73
w/o RL-AD	12.50	42.08	19.17	10.11
w/o TG	5.00	48.33	9.17	4.17
APEX	13.33	54.59	20.00	10.14

parameter balances the agent’s tendency between exploitation and exploration (Eq. (13)). As shown in Tab. 3, we evaluate various values for α . The results indicate that an α of 0.2 achieves the best overall performance, striking an optimal balance between attraction and exploration rewards.

Next, we analyze the necessity of each core module, with results summarized in Tab. 4. To verify the function of the 3D Dynamic Grid-based Map, we removed it and used raw RGB and depth images as direct observational inputs to the Action Decision Module. The model struggled to converge under this setting and achieved poor navigation performance. To assess the impact of the RL-based Action Decision Module, we replaced it with a reward-prediction-based heuristic algorithm. The details of this algorithm can be seen in Appendix C. Although this heuristic achieved acceptable results, its tendency to get trapped in local optima led to performance that was inferior to our original module. Finally, to demonstrate the importance of the Target Grounding Module, we replaced it with a simple rule to navigate towards the highest activation point in the attraction map, which led to a substantial drop in performance and underscored the necessity of our specialized mechanism for accurate target localization.

5. Conclusion

In this study, we introduced APEX (Aerial Parallel Explorer), a novel agent for Aerial Object Goal Navigation. APEX features a hierarchical architecture consisting of three specialized modules: Dynamic Spatio-Semantic Mapping Module, RL-based Decision Making module, and Target Grounding module. These components are efficiently

integrated through a novel Asynchronous Parallel Framework. Experimental results on the UAV-ON Benchmark demonstrate that APEX not only achieves state-of-the-art performance but also exhibits superior reliability and higher operational efficiency. In the future, we will conduct further research and optimization, including fine-tuning pre-trained VLM and MLLM models specifically for the Aerial Object-Nav task, as well as comparing the effects of different novel RL methods on APEX.

References

- [1] Peter Anderson, Angel X. Chang, Devendra Singh Chaplot, Alexey Dosovitskiy, Saurabh Gupta, Vladlen Koltun, Jana Kosecka, Jitendra Malik, Roozbeh Mottaghi, Manolis Savva, and Amir R. Zamir. On evaluation of embodied navigation agents. *CoRR*, abs/1807.06757, 2018. [3](#)
- [2] Peter Anderson, Qi Wu, Damien Teney, Jake Bruce, Mark Johnson, Niko Sünderhauf, Ian D. Reid, Stephen Gould, and Anton van den Hengel. Vision-and-language navigation: Interpreting visually-grounded navigation instructions in real environments. In *2018 IEEE Conference on Computer Vision and Pattern Recognition, CVPR 2018, Salt Lake City, UT, USA, June 18-22, 2018*, pages 3674–3683. Computer Vision Foundation / IEEE Computer Society, 2018. [3](#)
- [3] Shuai Bai, Keqin Chen, Xuejing Liu, Jialin Wang, Wenbin Ge, Sibo Song, Kai Dang, Peng Wang, Shijie Wang, Jun Tang, Humen Zhong, Yuanzhi Zhu, Ming-Hsuan Yang, Zhaohai Li, Jianqiang Wan, Pengfei Wang, Wei Ding, Zheren Fu, Yiheng Xu, Jiabo Ye, Xi Zhang, Tianbao Xie, Zesen Cheng, Hang Zhang, Zhibo Yang, Haiyang Xu, and Junyang Lin. Qwen2.5-vl technical report. *CoRR*, abs/2502.13923, 2025. [4](#), [7](#)
- [4] Hengxing Cai, Jinhan Dong, Jingjun Tan, Jingcheng Deng, Sihang Li, Zhifeng Gao, Haidong Wang, Zicheng Su, Agachai Sumalee, and Renxin Zhong. Flightgpt: Towards generalizable and interpretable UAV vision-and-language navigation with vision-language models. *CoRR*, abs/2505.12835, 2025. [2](#), [3](#)
- [5] Angel X. Chang, Angela Dai, Thomas A. Funkhouser, Maciej Halber, Matthias Nießner, Manolis Savva, Shuran Song, Andy Zeng, and Yinda Zhang. Matterport3d: Learning from RGB-D data in indoor environments. In *2017 International Conference on 3D Vision, 3DV 2017, Qingdao, China, October 10-12, 2017*, pages 667–676. IEEE Computer Society, 2017. [3](#)
- [6] Meng Chu, Zhedong Zheng, Wei Ji, Tingyu Wang, and Tat-Seng Chua. Towards natural language-guided drones: Geotext-1652 benchmark with spatial relation matching. In *Computer Vision - ECCV 2024 - 18th European Conference, Milan, Italy, September 29-October 4, 2024, Proceedings, Part XI*, pages 213–231. Springer, 2024. [2](#)
- [7] Zhengru Fang, Zhenghao Liu, Jingjing Wang, Senkang Hu, Yu Guo, Yiqin Deng, and Yuguang Fang. Task-oriented communications for visual navigation with edge-aerial collaboration in low altitude economy. *CoRR*, abs/2504.18317, 2025. [3](#)
- [8] Yunpeng Gao, Chenhui Li, Zhongrui You, Junli Liu, Zhen Li, Pengan Chen, Qizhi Chen, Zhonghan Tang, Liansheng Wang, Penghui Yang, Yiwen Tang, Yuhang Tang, Shuai Liang, Songyi Zhu, Ziqin Xiong, Yifei Su, Xinyi Ye, Jianan Li, Yan Ding, Dong Wang, Zhigang Wang, Bin Zhao, and Xuelong Li. Openfly: A versatile toolchain and large-scale benchmark for aerial vision-language navigation. *CoRR*, abs/2502.18041, 2025. [1](#)
- [9] Akash Ghosh, Arkadeep Acharya, Sriparna Saha, Vinija Jain, and Aman Chadha. Exploring the frontier of vision-language models: A survey of current methodologies and future directions. *CoRR*, abs/2404.07214, 2024. [1](#)
- [10] Jing Gu, Eliana Stefan, Qi Wu, Jesse Thomason, and Xin Wang. Vision-and-language navigation: A survey of tasks, methods, and future directions. In *Proceedings of the 60th Annual Meeting of the Association for Computational Linguistics (Volume 1: Long Papers), ACL 2022, Dublin, Ireland, May 22-27, 2022*, pages 7606–7623. Association for Computational Linguistics, 2022. [1](#)
- [11] Yukai Hou, Jin Zhao, Rongqing Zhang, Xiang Cheng, and Liuqing Yang. UAV swarm cooperative target search: A multi-agent reinforcement learning approach. *IEEE Trans. Intell. Veh.*, 9(1):568–578, 2024. [3](#)
- [12] Yatai Ji, Zhengqiu Zhu, Yong Zhao, Beidan Liu, Chen Gao, Yihao Zhao, Sihang Qiu, Yue Hu, Quanjun Yin, and Yong Li. Towards autonomous UAV visual object search in city space: Benchmark and agentic methodology. *CoRR*, abs/2505.08765, 2025. [3](#)
- [13] Minwoo Kim, Geun Sik Bae, Jinwoo Lee, Woojae Shin, Changseung Kim, Myong-Yol Choi, Heejung Shin, and Hyondong Oh. RAPID: robust and agile planner using inverse reinforcement learning for vision-based drone navigation. *CoRR*, abs/2502.02054, 2025. [3](#)
- [14] Seungchan Kim, Omar Alama, Dmytro Kurdydyk, John Keller, Nikhil Varma Keetha, Wenshan Wang, Yonatan Bisk, and Sebastian A. Scherer. RAVEN: resilient aerial navigation via open-set semantic memory and behavior adaptation. *CoRR*, abs/2509.23563, 2025. [3](#)
- [15] Eric Kolve, Roozbeh Mottaghi, Daniel Gordon, Yuke Zhu, Abhinav Gupta, and Ali Farhadi. AI2-THOR: an interactive 3d environment for visual AI. *CoRR*, abs/1712.05474, 2017. [3](#)
- [16] Jacob Krantz, Erik Wijmans, Arjun Majumdar, Dhruv Batra, and Stefan Lee. Beyond the nav-graph: Vision-and-language navigation in continuous environments. In *Computer Vision - ECCV 2020 - 16th European Conference, Glasgow, UK, August 23-28, 2020, Proceedings, Part XXVIII*, pages 104–120. Springer, 2020. [3](#)
- [17] Jungdae Lee, Taiki Miyanishi, Shuhei Kurita, Koya Sakamoto, Daichi Azuma, Yutaka Matsuo, and Nakamasa Inoue. Citynav: Language-goal aerial navigation dataset with geographic information. *CoRR*, abs/2406.14240, 2024. [1](#)
- [18] Nianxin Li, Mao Ye, Lihua Zhou, Song Tang, Yan Gan, Zizhuo Liang, and Xiatian Zhu. Self-prompting analogical reasoning for UAV object detection. In *AAAI-25, Sponsored by the Association for the Advancement of Artificial Intelligence*

gence, February 25 - March 4, 2025, Philadelphia, PA, USA, pages 18412–18420. AAAI Press, 2025. 2

[19] Tianshun Li, Tianyi Huai, Zhen Li, Yichun Gao, Haoang Li, and Xinhua Zheng. Skyvln: Vision-and-language navigation and NMPC control for uavs in urban environments. *CoRR*, abs/2507.06564, 2025. 2, 3

[20] Yunxin Li, Zhenyu Liu, Zitao Li, Xuanyu Zhang, Zhenran Xu, Xinyu Chen, Haoyuan Shi, Shenyuan Jiang, Xintong Wang, Jifang Wang, Shouzheng Huang, Xinping Zhao, Borui Jiang, Lanqing Hong, Longyue Wang, Zhuotao Tian, Baoxing Huai, Wenhan Luo, Weihua Luo, Zheng Zhang, Baotian Hu, and Min Zhang. Perception, reason, think, and plan: A survey on large multimodal reasoning models. *CoRR*, abs/2505.04921, 2025. 3

[21] Zongxia Li, Xiyang Wu, Hongyang Du, Fuxiao Liu, Huy Nghiem, and Guangyao Shi. A survey of state of the art large vision language models: Benchmark evaluations and challenges. In *IEEE/CVF Conference on Computer Vision and Pattern Recognition Workshops, CVPR Workshops 2025, Nashville, TN, USA, June 11-15, 2025*, pages 1587–1606. Computer Vision Foundation / IEEE, 2025. 1

[22] Shoon Kit Lim, Melissa Chong Jia Ying, Jing Huey Khor, and Ting Yang Ling. Taking flight with dialogue: Enabling natural language control for px4-based drone agent. *CoRR*, abs/2506.07509, 2025. 2

[23] Fei Lin, Yonglin Tian, Tengchao Zhang, Jun Huang, Sangan Guan, and Fei-Yue Wang. Airvista-ii: An agentic system for embodied uavs toward dynamic scene semantic understanding. *CoRR*, abs/2504.09583, 2025. 2

[24] Shubo Liu, Hongsheng Zhang, Yuankai Qi, Peng Wang, Yan-ning Zhang, and Qi Wu. Aerialvln: Vision-and-language navigation for uavs. In *IEEE/CVF International Conference on Computer Vision, ICCV 2023, Paris, France, October 1-6, 2023*, pages 15338–15348. IEEE, 2023. 1, 3

[25] Shilong Liu, Zhaoyang Zeng, Tianhe Ren, Feng Li, Hao Zhang, Jie Yang, Qing Jiang, Chunyuan Li, Jianwei Yang, Hang Su, Jun Zhu, and Lei Zhang. Grounding DINO: marrying DINO with grounded pre-training for open-set object detection. In *Computer Vision - ECCV 2024 - 18th European Conference, Milan, Italy, September 29-October 4, 2024, Proceedings, Part XLVII*, pages 38–55. Springer, 2024. 4, 6

[26] Youzhi Liu, Fanglong Yao, Yuanchang Yue, Guangluan Xu, Xian Sun, and Kun Fu. Navagent: Multi-scale urban street view fusion for UAV embodied vision-and-language navigation. *CoRR*, abs/2411.08579, 2024. 2, 3

[27] Artem Lykov, Valerii Serpiva, Muhammad Haris Khan, Oleg Sautenkov, Artyom Myshlyav, Grik Tadevosyan, Yasheerah Yaqoot, and Dzmitry Tsetserukou. Cognitivedrone: A VLA model and evaluation benchmark for real-time cognitive task solving and reasoning in uavs. *CoRR*, abs/2503.01378, 2025. 2

[28] Alec Radford, Jong Wook Kim, Chris Hallacy, Aditya Ramesh, Gabriel Goh, Sandhini Agarwal, Girish Sastry, Amanda Askell, Pamela Mishkin, Jack Clark, Gretchen Krueger, and Ilya Sutskever. Learning transferable visual models from natural language supervision. In *Proceedings of the 38th International Conference on Machine Learning, ICML 2021, 18-24 July 2021, Virtual Event*, pages 8748–8763. PMLR, 2021. 7

[29] Antonin Raffin, Ashley Hill, Adam Gleave, Anssi Kanervisto, Maximilian Ernestus, and Noah Dormann. Stable-baselines3: Reliable reinforcement learning implementations. *J. Mach. Learn. Res.*, 22:268:1–268:8, 2021. 2

[30] Ram Ramrakhy, Dhruv Batra, Erik Wijmans, and Abhishek Das. Pirlnav: Pretraining with imitation and RL finetuning for OBJECTNAV. In *IEEE/CVF Conference on Computer Vision and Pattern Recognition, CVPR 2023, Vancouver, BC, Canada, June 17-24, 2023*, pages 17896–17906. IEEE, 2023. 3

[31] Tianhe Ren, Shilong Liu, Ailing Zeng, Jing Lin, Kun-chang Li, He Cao, Jiayu Chen, Xinyu Huang, Yukang Chen, Feng Yan, Zhaoyang Zeng, Hao Zhang, Feng Li, Jie Yang, Hongyang Li, Qing Jiang, and Lei Zhang. Grounded SAM: assembling open-world models for diverse visual tasks. *CoRR*, abs/2401.14159, 2024. 4

[32] Ranjan Sapkota, Konstantinos I. Roumeliotis, and Manoj Karkee. Uavs meet agentic AI: A multidomain survey of autonomous aerial intelligence and agentic uavs. *CoRR*, abs/2506.08045, 2025. 1

[33] John Schulman, Filip Wolski, Prafulla Dhariwal, Alec Radford, and Oleg Klimov. Proximal policy optimization algorithms. *CoRR*, abs/1707.06347, 2017. 4, 7

[34] Valerii Serpiva, Artem Lykov, Artyom Myshlyav, Muhammad Haris Khan, Ali Alridha Abdulkarim, Oleg Sautenkov, and Dzmitry Tsetserukou. Racevla: Vla-based racing drone navigation with human-like behaviour. *CoRR*, abs/2503.02572, 2025. 2

[35] Yifei Su, Dong An, Kehan Chen, Weichen Yu, Baiyang Ning, Yonggen Ling, Yan Huang, and Liang Wang. Learning fine-grained alignment for aerial vision-dialog navigation. In *AAAI-25, Sponsored by the Association for the Advancement of Artificial Intelligence, February 25 - March 4, 2025, Philadelphia, PA, USA*, pages 7060–7068. AAAI Press, 2025. 3

[36] Xingpeng Sun, Zherong Pan, Xifeng Gao, Kui Wu, and Aniket Bera. Text-guided generation of efficient personalized inspection plans. *CoRR*, abs/2506.02917, 2025. 3

[37] Zhichao Sun, Yepeng Liu, Huachao Zhu, Yuliang Gu, Yuda Zou, Zelong Liu, Gui-Song Xia, Bo Du, and Yongchao Xu. Refdrone: A challenging benchmark for referring expression comprehension in drone scenes. *CoRR*, abs/2502.00392, 2025. 2

[38] Yonglin Tian, Fei Lin, Yiduo Li, Tengchao Zhang, Qiyao Zhang, Xuan Fu, Jun Huang, Xingyuan Dai, Yutong Wang, Chunwei Tian, Bai Li, Yisheng Lv, Levente Kovács, and Feiyue Wang. Uavs meet llms: Overviews and perspectives towards agentic low-altitude mobility. *Inf. Fusion*, 122: 103158, 2025. 1

[39] Xiangyu Wang, Donglin Yang, Yue Liao, Wenhao Zheng, Wenjun Wu, Bin Dai, Hongsheng Li, and Si Liu. Uav-flow colosseo: A real-world benchmark for flying-on-a-word UAV imitation learning. *CoRR*, abs/2505.15725, 2025. 2

[40] Xiangyu Wang, Donglin Yang, Ziqin Wang, Hohin Kwan, Jinyu Chen, Wenjun Wu, Hongsheng Li, Yue Liao, and

Si Liu. Towards realistic UAV vision-language navigation: Platform, benchmark, and methodology. In *The Thirteenth International Conference on Learning Representations, ICLR 2025, Singapore, April 24-28, 2025*. OpenReview.net, 2025. 2, 3, 7

[41] Pengying Wu, Yao Mu, Bingxian Wu, Yi Hou, Ji Ma, Shanghang Zhang, and Chang Liu. Voronav: Voronoi-based zero-shot object navigation with large language model. In *Forty-first International Conference on Machine Learning, ICML 2024, Vienna, Austria, July 21-27, 2024*. OpenReview.net, 2024. 3

[42] Ruipu Wu, Yige Zhang, Jinyu Chen, Linjiang Huang, Shifeng Zhang, Xu Zhou, Liang Wang, and Si Liu. Aeroduo: Aerial duo for uav-based vision and language navigation. *CoRR*, abs/2508.15232, 2025. 2

[43] Wansen Wu, Tao Chang, Xinpeng Li, Quanjun Yin, and Yue Hu. Vision-language navigation: a survey and taxonomy. *Neural Comput. Appl.*, 36(7):3291–3316, 2024. 1

[44] Jianqiang Xiao, Yuexuan Sun, Yixin Shao, Boxi Gan, Rongqiang Liu, Yanjing Wu, Weili Guan, and Xiang Deng. UAV-ON: A benchmark for open-world object goal navigation with aerial agents. *CoRR*, abs/2508.00288, 2025. 2, 3, 6, 7

[45] Haotian Xu, Yue Hu, Chen Gao, Zhengqiu Zhu, Yong Zhao, Yong Li, and Quanjun Yin. Geonav: Empowering mllms with explicit geospatial reasoning abilities for language-goal aerial navigation. *CoRR*, abs/2504.09587, 2025. 2

[46] Brian Yamauchi. A frontier-based approach for autonomous exploration. In *Proceedings 1997 IEEE International Symposium on Computational Intelligence in Robotics and Automation CIRA'97 - Towards New Computational Principles for Robotics and Automation, July 10-11, 1997, Monterey, California, USA*, pages 146–151. IEEE Computer Society, 1997. 7

[47] Fanglong Yao, Yuanchang Yue, Youzhi Liu, Xian Sun, and Kun Fu. Aeroverse: Uav-agent benchmark suite for simulating, pre-training, finetuning, and evaluating aerospace embodied world models. *CoRR*, abs/2408.15511, 2024. 1

[48] Fanglong Yao, Youzhi Liu, Wenyi Zhang, Zhengqiu Zhu, Chenglong Li, Nayu Liu, Peng Hu, Yuanchang Yue, Kaiwen Wei, Xin He, Xudong Zhao, Zihan Wei, Haotian Xu, Zhiyuan Wang, Gujie Shao, Liu Yang, Dan Zhao, and Yong Yang. Aeroverse-review: Comprehensive survey on aerial embodied vision-and-language navigation. *The Innovation Informatics*, 1(1):100015, 2025. 1

[49] Shukang Yin, Chaoyou Fu, Sirui Zhao, Ke Li, Xing Sun, Tong Xu, and Enhong Chen. A survey on multimodal large language models. *CoRR*, abs/2306.13549, 2023. 3

[50] Bangguo Yu, Hamidreza Kasaei, and Ming Cao. L3MVN: leveraging large language models for visual target navigation. In *IROS*, pages 3554–3560, 2023. 7

[51] Jingyi Zhang, Jiaxing Huang, Sheng Jin, and Shijian Lu. Vision-language models for vision tasks: A survey. *IEEE Trans. Pattern Anal. Mach. Intell.*, 46(8):5625–5644, 2024. 1

[52] Weichen Zhang, Chen Gao, Shiquan Yu, Ruiying Peng, Baining Zhao, Qian Zhang, Jinqiang Cui, Xinlei Chen, and Yong Li. Citynavagent: Aerial vision-and-language navigation with hierarchical semantic planning and global memory. In *Proceedings of the 63rd Annual Meeting of the Association for Computational Linguistics (Volume 1: Long Papers), ACL 2025, Vienna, Austria, July 27 - August 1, 2025*, pages 31292–31309. Association for Computational Linguistics, 2025. 3

[53] Xinyuan Zhang, Yonglin Tian, Fei Lin, Yue Liu, Jing Ma, Kornélia Sára Szatmáry, and Fei-Yue Wang. Logisticsvln: Vision-language navigation for low-altitude terminal delivery based on agentic uavs. *CoRR*, abs/2505.03460, 2025. 2

[54] Yue Zhang, Ziqiao Ma, Jialu Li, Yanyuan Qiao, Zun Wang, Joyce Chai, Qi Wu, Mohit Bansal, and Parisa Kordjamshidi. Vision-and-language navigation today and tomorrow: A survey in the era of foundation models. *Trans. Mach. Learn. Res.*, 2024, 2024. 1

[55] Yuhang Zhang, Haosheng Yu, Jiaoping Xiao, and Mir Feroskhan. Grounded vision-language navigation for uavs with open-vocabulary goal understanding. *CoRR*, abs/2506.10756, 2025. 3

[56] Ganlong Zhao, Guanbin Li, Jia Pan, and Yizhou Yu. Aerial vision-and-language navigation with grid-based view selection and map construction. *CoRR*, abs/2503.11091, 2025. 2

[57] Ji Zhao and Xiao Lin. General-purpose aerial intelligent agents empowered by large language models. *CoRR*, abs/2503.08302, 2025. 2

[58] Shijin Zhao, Fuhui Zhou, and Qihui Wu. AAV visual navigation in the large-scale outdoor environment: A semantic-map-based cognitive escape reinforcement learning method. *IEEE Internet Things J.*, 12(11):15926–15938, 2025. 3

[59] Yifan Zhong, Fengshuo Bai, Shaofei Cai, Xuchuan Huang, Zhang Chen, Xiaowei Zhang, Yuanfei Wang, Shaoyang Guo, Tianrui Guan, Ka Nam Lui, Zhiqian Qi, Yitao Liang, Yuanpei Chen, and Yaodong Yang. A survey on vision-language-action models: An action tokenization perspective. *CoRR*, abs/2507.01925, 2025. 2

[60] Gengze Zhou, Yicong Hong, Zun Wang, Xin Eric Wang, and Qi Wu. Navgpt-2: Unleashing navigational reasoning capability for large vision-language models. In *Computer Vision - ECCV 2024 - 18th European Conference, Milan, Italy, September 29-October 4, 2024, Proceedings, Part VII*, pages 260–278. Springer, 2024. 3

APEX: A Decoupled Memory-based Explorer for Asynchronous Aerial Object Goal Navigation

Supplementary Material

6. Algorithm Flow

Algorithm 1 and Algorithm 2 illustrates the overall workflow of our agent. We employ a multi-process architecture to enable parallel execution of the three modules.

Algorithm 1 Overall Workflow

Input: Observations O

Input: States S

Input: Target Description D

- MEM denotes the shared information, including M_{attr} , M_{expl} , M_{obst} , and others.

```
1: function MAP UPDATING( $MEM, O, S, D$ )
2:   while not IsDetected do
3:      $c, s \leftarrow CAP(O, D)$ 
4:      $\mathcal{M} \leftarrow SEG(O, c)$ 
5:      $MEM \leftarrow \text{Update}(MEM, \mathcal{M}, s, O, S)$ 
6:   end while
7:   process.join()
8: end function

9: function ACTION DECISION( $MEM, S, O, p$ )
10:  while True do
11:    if IsDetected then
12:      Navigate( $p$ )
13:    else
14:      break
15:    end if
16:     $MEM \leftarrow \text{Update}(MEM, O, S)$ 
17:     $a \leftarrow \text{Policy}(MEM, S)$ 
18:    Execute( $a$ )
19:  end while
20:  process.join()
21: end function

22: function TARGET GROUNDING
23:   while not IsDetected do
24:      $b \leftarrow GD(O, D)$ 
25:      $p \leftarrow RP(b, O, S)$ 
26:   end while
27:   process.join()
28: end function
```

7. More Visualization Results

7.1. Cases

We provide additional visualizations to further illustrate APEX’s performance. Fig. 8 shows four navigation episodes: three successful searches for ”Car”, ”Playground”, and ”Umbrella”, and one failure case targeting a ”Sandbox”. The failure was caused by a collision with a tree, which suggests a potential limitation in our Obstacle Map’s ability to detect sparse obstacles.

7.2. Trajectories

Fig. 6 demonstrates the complete trajectories for these four cases (labeled as Case 1-4), in addition to the main paper’s example (Case 0).

8. Details of Heuristic Algorithm

The heuristic algorithm mentioned in Ablation Study is detailed in Algorithm 3. The core idea is to simulate each possible action, evaluate the potential reward based on attraction and exploration criteria, and select the action with the highest predicted reward.

9. More Training Details

9.1. Offline Map Generation

Directly incorporating the VLM for attraction map generation within the reinforcement learning loop is infeasible due to its high inference latency. To address this, we pre-generate a complete attraction map for each of the 36 tasks before training begins, which are shown in Fig. 7.

For each task, we designed a flight path to cover the entire relevant search area. An agent was simulated along this path to generate and store a full attraction map. During RL training, instead of calling the VLM, the agent identifies its currently visible grid cells via the depth map and populates its local attraction map by looking up the pre-computed values. This method bypasses the VLM’s latency, making the RL training process computationally available.

9.2. Policy Network Architecture

Fig. 5 illustrates the architecture of the policy network in our RL-based Action Decision Module. It utilizes three CNNs to extract features from the Attraction, Exploration, and Obstacle maps, respectively. To process the 3D map data, the z-axis is treated as the channel dimension for the

Algorithm 2 Memory Updating Workflow

Input: Masks \mathcal{M}
Input: Observations O
Input: States S
Input: Attraction Scores s

```

1: function ATTRUPDATE( $M_{\text{attr}}$ ,  $s$ ,  $\mathcal{M}$ ,  $O$ ,  $S$ )
2:    $\mathcal{G}_{\text{vis}}$ : the set of visible grid cells in the current view.
3:   for  $g \in \mathcal{G}_{\text{vis}}$  do
4:      $P_g$ : the set of pixels from  $O$  that project to  $g$ .
5:      $Mask^* \leftarrow \arg \max_{Mask_i \in \mathcal{M}} |P_g \cap Mask_i|$ 
6:     if  $Mask^*$  is found then
7:        $s^* \leftarrow$  score in  $s$  corresponding to  $Mask^*$ 
8:        $d_{\text{new}} \leftarrow \text{Dis}(S.\text{pos}, g.\text{center})$ 
9:       if  $d_{\text{new}} < M_{\text{attr}}[g].\text{dis}$  then
10:         $M_{\text{attr}}[g].\text{score} \leftarrow s^*$ 
11:         $M_{\text{attr}}[g].\text{dis} \leftarrow d_{\text{new}}$ 
12:      end if
13:    end if
14:   end for
15:   return  $M_{\text{attr}}$ 
16: end function

17: function EXPLUPDATE( $M_{\text{expl}}$ ,  $O$ ,  $S$ )
18:    $\mathcal{P}_{\text{end}}$ : the set of 3D world points from  $O$ .
19:    $\mathcal{G}_{\text{traversed}} \leftarrow \text{TraceRay}(S.\text{pos}, \mathcal{P}_{\text{end}})$ 
20:   for  $g \in \mathcal{G}_{\text{traversed}}$  do
21:      $d \leftarrow \text{distance}(S.\text{pos}, g.\text{center})$ 
22:      $v_{\text{current}} \leftarrow M_{\text{expl}}[g]$ 
23:      $v_{\text{new}} \leftarrow \text{ExplRate}(d, v_{\text{current}})$ 
24:      $M_{\text{expl}}[g] \leftarrow v_{\text{current}} + v_{\text{new}}$ 
25:   end for
26:   return  $M_{\text{expl}}$ 
27: end function

28: function OBSTUPDATE( $M_{\text{obst}}$ ,  $O$ ,  $S$ )
29:    $\mathcal{G}_{\text{depth}}$ : the set of grid cells hit by depth rays from  $O$ .
30:    $M_{\text{obst}}[g] \leftarrow 1, \quad \forall g \in \mathcal{G}_{\text{depth}}$ 
31:   return  $M_{\text{obst}}$ 
32: end function

33: function TRACERAY( $S_{\text{start}}$ ,  $\mathcal{P}_{\text{end}}$ )
34:    $\mathcal{G}_{\text{traversed}}$ : the set of grid cells
35:   for  $p_{\text{end}} \in \mathcal{P}_{\text{end}}$  do
36:      $\vec{r} = p_{\text{end}} - S_{\text{start}}$ 
37:     Sample points  $\mathcal{P}_s$  along  $\vec{r}$  at regular intervals.
38:      $\mathcal{G}_{\text{traversed}} \leftarrow \text{RP}(\mathcal{P}_s)$ 
39:   end for
40:   return  $\mathcal{G}_{\text{traversed}}$ 
41: end function

```

Algorithm 3 Heuristic Action Decision

Input: Attraction Map M_{attr}
Input: Exploration Map M_{expl}
Input: Obstacle Map M_{obst}
Input: Current State s

- Let a be an action from the action set \mathcal{A} .
- Let s' be the hypothetical state after action a .
- The **attraction reward** R_{attr} and **exploration reward** R_{expl} is defined in main paper.

```

1: Initialize  $R$  to store the predicted reward.
2: for  $a \in \mathcal{A}$  do
3:    $s' \leftarrow \text{Simulate}(a, s, M_{\text{attr}}, M_{\text{expl}}, M_{\text{obst}})$ 
4:   if IsUnsafe( $s'$ ) then
5:      $R[a] \leftarrow -\infty$ 
6:   continue
7:   else
8:      $R[a] \leftarrow W_{\text{attr}}R_{\text{attr}}(s') + W_{\text{expl}}R_{\text{expl}}(s')$ 
9:   end if
10: end for
11: return  $\arg \max_{a \in \mathcal{A}} R[a]$ 

```

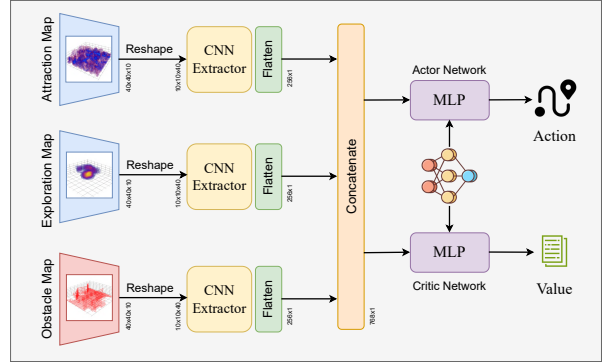


Figure 5. The architecture of policy network.

convolutional layers. The resulting feature vectors are concatenated and shared between an Actor (MLP) and a Critic (MLP) head. The Actor network outputs the final action policy. This implementation is based on the MultiInputPolicy architecture provided by the Stable-Baselines3 [29].

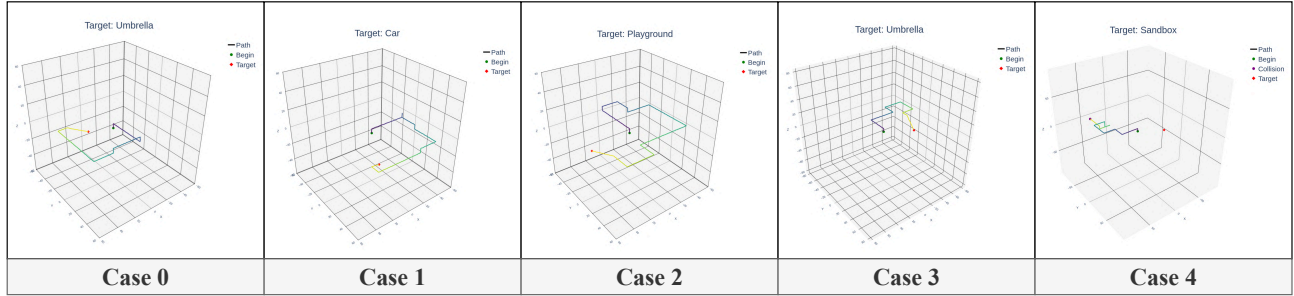


Figure 6. Complete trajectories of visualization examples.

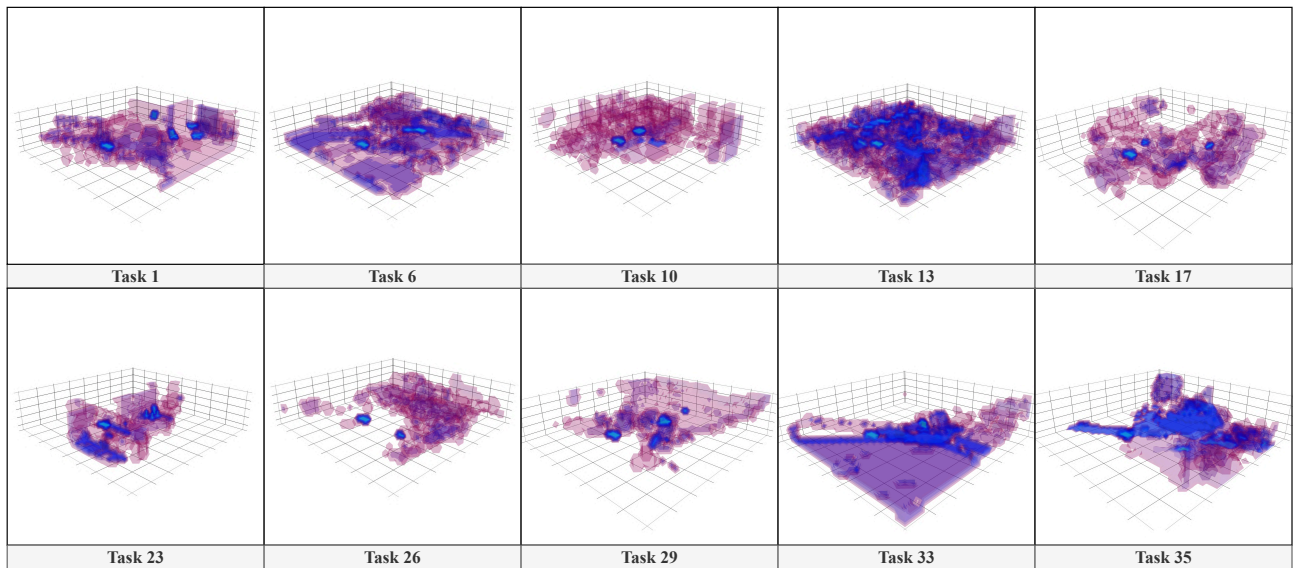


Figure 7. Examples of collected attraction maps.



Figure 8. More visualized results. The first three examples are successful cases, with the targets "Car", "Playground", and "Umbrella" respectively. The last one is a failure case, with the target being "Sandbox".